

# High-speed varifocal imaging with a tunable acoustic gradient index of refraction lens

Alexandre Mermillod-Blondin, Euan McLeod, and Craig B. Arnold\*

Department of Mechanical and Aerospace Engineering, Princeton University, 1 Olden Street,  
Princeton, New Jersey 08544, USA

\*Corresponding author: cbarnold@princeton.edu

Received June 5, 2008; accepted July 16, 2008;  
posted August 21, 2008 (Doc. ID 96974); published September 12, 2008

Fluidic lenses allow for varifocal optical elements, but current approaches are limited by the speed at which focal length can be changed. Here we demonstrate the use of a tunable acoustic gradient (TAG) index of refraction lens as a fast varifocal element. The optical power of the TAG lens varies continuously, allowing for rapid selection and modification of the effective focal length at time scales of 1  $\mu$ s and shorter. The wavefront curvature applied to the incident light is experimentally quantified as a function of time, and single-frame imaging is demonstrated. Results indicate that the TAG lens can successfully be employed to perform high-rate imaging at multiple locations. © 2008 Optical Society of America

OCIS codes: 110.1080, 220.1080, 230.1040.

The ability to rapidly change the focal plane of an optical system has applications in various fields, such as confocal profilometry [1], confocal microscopy [2], focus tracking [3], or material processing [4]. For all these practical uses, a fast focal-scanning optical element with a high transmission coefficient is desirable but is not readily available.

Dynamic focal scanning can be performed by mechanical translation of an ensemble of optical elements [5] or by the use of reconfigurable liquid-crystal-based modulators [6] or membrane mirrors [3]. Additionally, adaptive liquid lenses based on changing the curvature of a surface or interface offer an interesting solution for varifocal applications, particularly for small-scale devices [7]. Although these technological options continue to be improved, they remain relatively limited in speed, with the best focal-scanning rates approximately in the kilohertz (kHz) range. Faster alternatives have been reported to operate at several hundreds of kHz. For instance, electro-optic lenses [8] and lenses based on acousto-optic crystals [1] have a response up to 400 kHz. As a main drawback, electro-optic lenses are polarization sensitive, and acousto-optic crystals have a weak transmission efficiency, owing to their need of multiple crystals for focusing a beam.

Recently, TAG lenses emerged as a new generation of high-speed tunable optical components able to provide complex beam profiles, such as Bessel beams [9,10]. By synchronizing the TAG lens with a pulsed light source, it was shown that one can rapidly select between specific patterns as annular or focused beams for materials processing [11]. In this Letter, we demonstrate how a TAG lens can be used as a fast varifocal converging or diverging simple lens with switching times faster than 1  $\mu$ s. The time-resolved wavefront is measured, and direct imaging through the TAG lens is demonstrated.

The TAG lens consists of a cylindrical piezoelectric shell filled with a transparent material. When the piezoelectric transducer (PZT) is driven with a sinusoidal voltage with frequency  $\omega$  in the rf range, a

standing-pressure wave periodically alters the refractive index distribution  $n(r, t)$  inside the refractive medium according to [12,13]

$$n(r, t) = n_0 + n_a J_0\left(\frac{\omega r}{v}\right) \sin(\omega t), \quad (1)$$

where  $n_0$  and  $v$  correspond to the static refractive index and to the speed of sound in the acoustic medium, respectively. The constant  $n_a$  depends on  $\omega$ , the physical properties of the acoustic medium, (the initial refractive index, the speed of sound, and the effective kinematic viscosity), and the peak inner-wall velocity (linearly proportional to the amplitude of the driving signal). For the conditions shown in this Letter,  $n_a \approx 10^{-5}$  [12]. Keeping the second-order term in the expansion of Eq. (1) in the vicinity of the optical axis gives

$$n(r, t) = n_0 + \left(n_a - \frac{n_a \omega^2}{4v^2} r^2\right) \sin(\omega t). \quad (2)$$

By identification with the transfer function of a lens, the effective lens power  $\delta(t)$  for the TAG lens can be written as

$$\delta(t) = \frac{1}{f(t)} = \frac{Ln_a \omega^2}{2v^2} \sin(\omega t), \quad (3)$$

where  $f(t)$  corresponds to the effective focal length and  $L$  is the length of the TAG lens (2.5 cm).

We measure time-resolved lens power  $\delta(t)$  using the stroboscopic wavefront analysis shown in Fig. 1. The laser source delivers 15 ns pulses at a wavelength of 355 nm and a diameter of 3.5 mm at  $1/e^2$ . We employ 0.65 cS silicone oil as the transparent material in the TAG, with a refractive index of 1.37 and a speed of sound of 873.2 m s<sup>-1</sup>. For these experiments, a sinusoidal 388 kHz rf signal drives the TAG lens at an eigenmode of the chamber. This signal is maintained constant, while a pulse-delay generator is used to trigger the laser with an arbitrary lag time

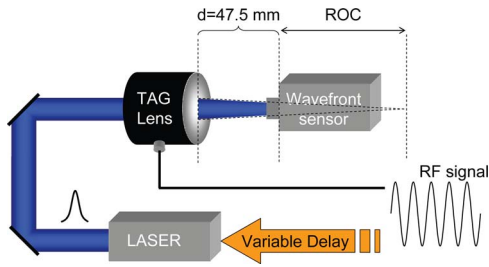


Fig. 1. (Color online) Experimental setup for determining the wavefront's ROC using a Shack–Hartmann sensor. The variable delay between the laser pulse and the ac driving signal is set with a pulse-delay generator.

relative to the TAG driving signal. This allows us to synchronize each pulse of light with the desired vibration state of the lens. The wavefront modulations experienced by the incoming laser beam are analyzed with a Shack–Hartmann wavefront sensor (Thorlabs WFS 150 C) placed 47.5 mm after the TAG lens output window. By limiting the size of the entrance pupil of the wavefront sensor to 1.6 mm, we make sure that only the wavefront distortions experienced by the central part of the laser beam are analyzed.

The wavefront sensor provides the radius of curvature (ROC) of the beam after the TAG lens. For a Gaussian beam, the relation between the lens power  $\delta$  and the ROC depends on the distance  $d$  between the lens and sensor according to

$$\frac{1}{ROC(d)} = \frac{-\delta^{-1} + d \left(1 + \frac{\delta^{-2}}{z_l^2}\right)}{(\delta^{-1} - d)^2 + \left(\frac{d\delta^{-1}}{z_l}\right)^2}, \quad (4)$$

where  $z_l$  is the Rayleigh range of the laser beam incident on the TAG lens.

Figure 2(a) shows that the lens power for the TAG lens operating in the steady state exhibits a sinusoidal oscillation at the frequency of the driving signal. It is possible to sample any lens power over the available range using a pulsed-light source or a high-speed camera, thereby enabling a fast varifocal lens. For the data shown, a driving amplitude of  $3.44 V_{p-p}$  allows the optical power of the TAG lens to vary between  $\delta_{min} = -1.6 \text{ m}^{-1}$  and  $\delta_{max} = 1.6 \text{ m}^{-1}$  in a time  $\Delta t = \pi/\omega = 1.3 \mu\text{s}$ . As expected from Eq. (2), the amplitude of the lens power varies linearly with respect to the amplitude of the driving signal, as shown in Fig. 2(b).

Figure 2(c) shows the relative amplitude of the Zernike modes fitting the smallest positive ROC wavefront when the amplitude of the driving signal is  $16.4 V_{p-p}$ . Modes (0,0) and (1,  $\pm 1$ ) are not plotted, as they represent the piston, tip, and tilt resulting from alignment between the lens and detector. The comparison of the amplitudes of the higher-order Zernike modes indicates that the output wavefront can be primarily fit by Zernike mode (2,0), corresponding to beam (de)focusing. The amplitudes of the higher modes are comparatively low, suggesting that the amount of aberrations introduced by the TAG lens is minimal.

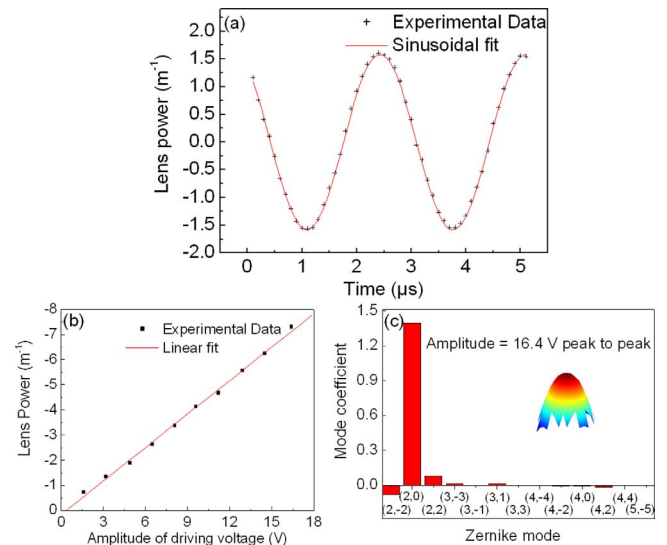


Fig. 2. (Color online) (a) TAG lens focusing power as a function of time for a  $3.44 V_{p-p}$  driving signal at a frequency of 388 kHz. The solid curve shows a two-parameter (amplitude and phase) sinusoidal fit to the data. (b) Maximum lens power as a function of the driving amplitude for the 388 kHz signal. The solid line shows a linear fit to the data. (c) Zernike mode coefficients fitting the wavefront of the output beam for a driving amplitude of  $16.4 V_{p-p}$ , a driving frequency of 388 kHz, and a synchronization delay set so that the lens power is maximized. The inset shows the reconstructed wavefront.

The low aberration associated with the TAG lens enables it to be used in imaging applications. Figure 3 shows such an experimental setup for imaging. A collimated spark lamp, producing 18 ns flashes of incoherent light, illuminates the object, which is a USAF 1951 calibration standard. We employ the same method as described in Fig. 1 to synchronize the spark lamp with the TAG lens. A 2.5 mm diameter iris is placed after the TAG lens in order to limit the effective aperture of the system to the region where the second-order expansion given in Eq. (2) remains valid. The imaging system consists of a CCD camera located at the focal plane of a 200 mm focal length lens (L) with the object placed at the focal length of the TAG. A sinusoidal signal  $16.4 V_{p-p}$  and 388 kHz drives the TAG lens.

When the TAG is off, the resolution standard is out of focus, as shown in Figs. 4(a) and 4(c). As the TAG is turned on, we can see the object is brought into focus and appears as a clean image on the CCD. By adjusting the relative phase delay between the lamp and the TAG lens, it is possible to select a desired

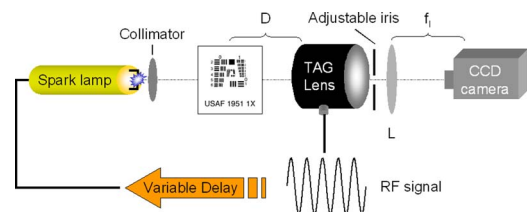


Fig. 3. (Color online) Experimental setup for imaging an object placed at a distance  $D$  before the TAG lens. The focal length of the fixed lens  $L$  is  $f_l = 200 \text{ mm}$ .

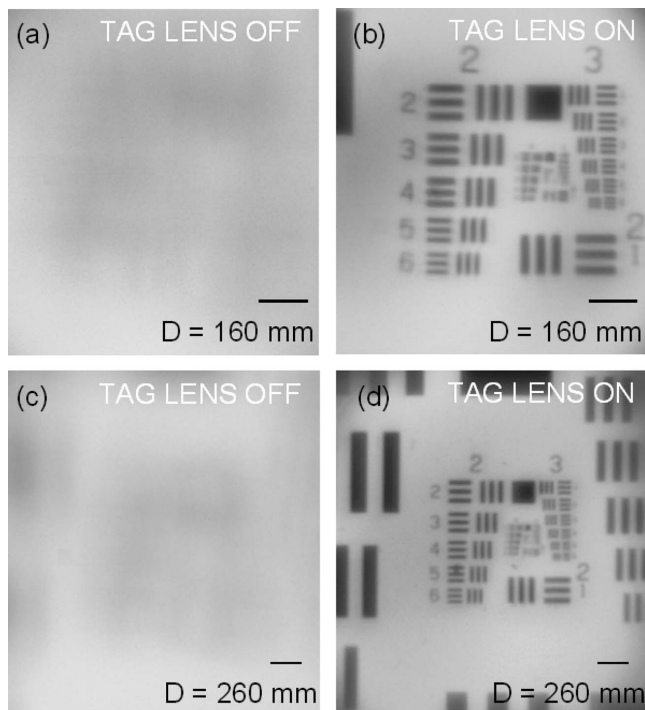


Fig. 4. Images of a USAF 1951 resolution test chart: (a) object at  $D = 160$  mm, TAG lens off; (b) object at  $D = 160$  mm, TAG lens on with the spark lamp synchronized so that the TAG lens focal length is 160 mm when the object is illuminated; (c) object at  $D = 260$  mm, TAG lens off; (d) object at  $D = 260$  mm, TAG lens on and synchronization set so that the TAG lens focal length is 260 mm. The time difference in the synchronization states of (b) and (d) is  $0.3 \mu\text{s}$ . The scale bars represent a 1 mm length.

lens power and establish the location of the object plane. In the case shown, placing an object at 160 mm away from the TAG represents the minimum object distance with the TAG operating at its maximum optical power. Changing the relative phase delay by  $t = 0.3 \mu\text{s}$  decreases the power, and the object plane is moved to 260 mm away from the TAG.

The results presented in Figs. 4(b) and 4(d) demonstrate that it is possible to switch the object plane over large distances from 160 to 260 in a minimum time of  $0.3 \mu\text{s}$ . The time to switch between two arbitrary planes is determined by the curve in Fig. 2(a).

However, the time to change from the minimum lens power to the maximum lens power is given by half the period of the driving signal.

In summary, we demonstrated that a TAG lens can be used as a fast reliable varifocal lens with switching times on the order of  $1 \mu\text{s}$ . The maximum range and minimum time for changing the lens power can be adjusted by simple electrical modifications to the driving signal. By combining the TAG lens with additional optical components, it is possible to apply the rapid focal plane scanning to many important imaging and focusing applications, such as those found in machine vision, scanning optical microscopy, or materials processing.

We thank Emmanuel Beaufrepaire for useful discussion on rapid imaging applications and the Air Force Office of Scientific Research (AFOSR) for financial support.

## References

1. A. Kaplan, N. Friedman, and N. Davidson, *Opt. Lett.* **26**, 1078 (2001).
2. L. Yang, A. M. Raighne, E. M. McCabe, A. L. Dunbar, and T. Scharf, *Appl. Opt.* **44**, 5928 (2005).
3. V. X. Yang, Y. Mao, B. A. Standish, N. R. Munce, S. Chiu, D. Burnes, B. C. Wilson, A. I. Vitkin, P. A. Himmer, and D. L. Dickensheets, *Opt. Lett.* **31**, 1262 (2006).
4. R. Kuwano, T. Tokunaga, Y. Otani, and N. Umeda, *Opt. Rev.* **12**, 405 (2005).
5. G. Druart, J. Taboury, N. Gurineau, R. Hadar, H. Sauer, A. Kattinig, and J. Primot, *Opt. Lett.* **33**, 366 (2008).
6. M. Ye, B. Wang, T. Takahashi, and S. Sato, *Opt. Rev.* **14**, 173 (2007).
7. S. Kuiper and B. H. W. Hendriks, *Appl. Phys. Lett.* **85**, 1128 (2004).
8. T. Shibaguchi and H. Funato, *Jpn. J. Appl. Phys.* **31**, 3196 (1992).
9. K. A. Higginson, M. A. Costolo, and E. A. Rietman, *Appl. Phys. Lett.* **84**, 843 (2004).
10. E. McLeod and C. B. Arnold, *Opt. Lett.* **31**, 3155 (2006).
11. A. Mermillod-Blondin, E. McLeod, and C. B. Arnold, *Appl. Phys. A* **93**, 231 (2008).
12. E. McLeod and C. B. Arnold, *J. Appl. Phys.* **102**, 033104 (2007).
13. I. Grulkowski, D. Jankowski, and P. Kwiek, *Appl. Opt.* **46**, 5870 (2007).